Rotational motion of BH_4 units in MBH_4 (M=Li,Na,K) from quasielastic neutron scattering and density functional calculations

Arndt Remhof,[1,*] Zbigniew Łodziana,[1,2] Pascal Martelli,[1] Oliver Friedrichs,[1] Andreas Züttel,[1] Alexander V. Skripov,[3] Jan Peter Embs,[4,†] and Thierry Strässle[4]

[1] *EMPA, Swiss Federal Laboratories for Materials Science and Technology, Hydrogen and Energy, Überlandstrasse 129, CH-8600 Dübendorf, Switzerland*

[2] *Institute of Nuclear Physics, Polish Academy of Sciences, ul. Radzikowskiego 152, PL-31-342 Kraków, Poland*

[3] *Institute of Metal Physics, Ural Division, Russian Academy of Sciences, S. Kovalevskoi 18, Ekaterinburg 620041, Russia*

[4] *Laboratory for Neutron Scattering, Paul Scherrer Institut, ETH Zurich, CH-5232 Villigen, Switzerland*

(Received 29 March 2010; revised manuscript received 10 May 2010; published 15 June 2010)

We present a combined experimental and theoretical study on the rotational motion of the $(BH_4)^-$ ions in alkaline tetrahydroborides MBH_4, M=(Li,Na,K). The BH_4 motions are thermally activated and characterized by activation energies in the order of 0.1 eV, typical frequencies are in the terahertz range at temperatures of about 400 K. In the cubic $NaBH_4$ and KBH_4 phases and in the high-temperature phase of $LiBH_4$, the motion of the $(BH_4)^-$ ion is dominated by 90° reorientations while it displays a threefold jump behavior in the low-temperature phase of $LiBH_4$. The experimental results are discussed on the basis of density functional theory calculations, revealing the potential-energy landscape of a $(BH_4)^-$ subunit in the crystalline matrix and relating the hydrogen dynamics to the structural properties of the respective compounds.

DOI: 10.1103/PhysRevB.81.214304 PACS number(s): 63.20.Pw, 88.30.rd, 29.30.Hs

I. INTRODUCTION

Alkaline tetrahydroborides are ionic crystals consisting of negatively charged $(BH_4)^-$ ions and positively charged M^+ metal ions, where M=(Li,Na,K,Rb,Cs). Apart from their classical application as reducing agents or as starting compounds for the synthesis of organometallic derivatives, the light-weight $LiBH_4$ and $NaBH_4$ are recently discussed as synthetic fuels either in the direct borohydride fuel cell[1] or as hydrogen storage materials for mobile applications.[2]

In alkaline borohydrides the hydrogen is covalently bound and arranged in subunits (complexes).[2] The four hydrogen atoms surrounding the central boron atom form a regular tetrahedron. The B-H distance is almost independent on the metal ion and from the actual crystal structure. At room temperature $d_{B\text{-}D}$=1.18–1.20 Å have been observed for the B-D distance in $LiBD_4$,[3] $d_{B\text{-}D}$=1.178 Å in $NaBD_4$ (Ref. 4), and $d_{B\text{-}D}$=1.196 Å in KBD_4.[5] Similar values have been found for $CsBH_4$, $RbBD_4$ (Ref. 5) and for $Ca(BH_4)_2$.[6] To visualize the geometry of the tetrahedron and its symmetry, it is helpful to regard it as being embedded inside a cube with an edge length of $a=\sqrt{4/3}d_{B\text{-}H}$ as displayed in Fig. 1. Thereby each vertex of the tetrahedron is a vertex of the cube, and each edge is a diagonal of one of the cube's faces. Two sets of high-symmetry axes are related to this structural arrangement. First, there are three twofold axes, called $c2$, which are normal to the cube's face and four threefold axes, called $c3$, which coincide with the body diagonals of the cube. Both symmetry operations map the tetrahedron to itself. There are two possibilities to match the four vertices of a tetrahedron to the eight vertices of the cube. These two possible arrangements may be transferred in one another by a 90° rotation around a $c2$ axis while a rotation around $c3$ preserves the tetrahedron's orientation.

It is generally believed that at ambient conditions the borohydrides of the monovalent alkali metals crystallize in a cubic NaCl-like structure. Details of the structures are, however, still subject of current research, especially for the case of $NaBH_4$.[4,7–9] In any of the cubic structure under discussion, the symmetry axes of the BH_4 tetrahedron coincide with the low index crystallographic axes. The $c2$ axes are thereby aligned with the [100] axes while the $c3$ axes lie along the [111] axis, which are the body diagonals of the cubic lattice. $LiBH_4$ is an exception to this rule. It crystallizes at room temperature in the orthorhombic *Pnma* structure (space group no. 62).[3,10] Heat-capacity studies for the MBH_4 series with M=Na,K,Rb,Cs suggest phase transitions at 190 K for $NaBH_4$, 76 K for KBH_4, 44 K for $RbBH_4$, and 27 K for $CsBH_4$, respectively.[11] The low-temperature (LT) phases of $NaBH_4$ and KBH_4 have been determined to be ordered tetragonal structures, where one of the BH_4 orientations is "frozen."[4,5] In the case of $RbBH_4$ and $CsBH_4$ no diffraction evidence for a lowering of structural symmetry has been found.[5] $LiBH_4$ undergoes a structural phase transition to a hexagonal high-temperature (HT) structure at around 380 K.[12] Diffraction studies have pointed out a dramatic increase in hydrogen or deuterium thermal displacements by almost 2 orders of magnitude from 4 to 400 K,[3,10] which was attributed to dynamical disorder in the HT phase.[13,14] The rotation of the BH_4 subunits is not restricted to $LiBH_4$, it has also been observed for $NaBH_4$ and KBH_4.[9]

In a combined experimental and theoretical study we examine the rotational motion of the BH_4 tetrahedra in $LiBH_4$, $NaBH_4$, and KBH_4 by means of quasielastic neutron scattering (QENS), inelastic neutron scattering (INS), and density functional theory (DFT) calculations. We identify the axes of rotation and relate them to the symmetry of the respective crystals. The experimentally obtained activation energies and residence times for BH_4 rotations, as well as the phonon density of states (PDOS) are determined by the spatial arrangement of the constituent atoms and are discussed in view of theoretical calculations.

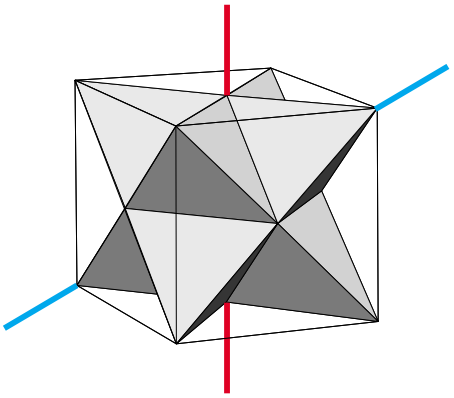

FIG. 1. (Color online) Two possible ways to embed a tetrahedron into a cube: each vertex of a tetrahedron is a vertex of the cube, each edge is a diagonal of one of the cube's faces. The two dual tetrahedra are plotted in two different shades of gray. A representative twofold $c2$ axis (normal to the cube's faces) and a representative threefold $c3$ axis (along the cubes' spatial diagonal) are indicated as well.

II. METHODS

A. Experimental

QENS and INS measurements were carried out using the time-of-flight (TOF) neutron spectrometer FOCUS for cold neutrons located at the continuous spallation source SINQ at the Paul Scherrer Institute in Villigen, Switzerland.[15,16] At the setting used, the elastic-scattering energy resolution, ΔE, was 0.20 meV, for incident neutrons with a wavelength of 4 Å and 0.06 meV for incident neutrons with a wavelength of 6 Å, respectively. The 6 Å setting was used for the examination of the $LiBH_4$ at temperatures below 350 K, all other measurements were carried out using the 4 Å setting. Isotopically enriched ^{11}B (99.5%) samples (chemical purity >98%), purchased from Katchem, were used to avoid the strong neutron absorption by natural boron. Due to the large incoherent neutron-scattering cross section of hydrogen, the quasielastic and inelastic signals are dominated by the hydrogen signal. The inelastic measurements were carried out in neutron energy gain mode; therefore at the measured temperatures, energies up to 60 meV were reasonably accessible. In order to obtain the PDOS from the inelastic spectra, the TOF data were corrected for the $1/\omega$ term, the polarization factor, the Bose-Einstein statistics for the thermal population, the Debye-Waller factor, and for the quasielastic contribution at low Q. The uncertainties, especially in the Debye-Waller factor are expressed by the error bars in Fig. 6(a).

To extract the QENS spectra data reduction was carried out using the data analysis and visualization environment "DAVE."[17] The spectra were binned in a range of scattering vectors of $Q=0.5-2.5$ Å^{-1}. The resulting QENS spectra were analyzed using the general purpose curve fitting utility "PAN," which is included in the DAVE distribution. All QENS spectra were modeled using two components: first, the elastic peak of width w_{el} and an integrated area I_{el}. The width of the elastic line was fixed to the width of the measured elastic line of a vanadium standard sample, corresponding to the instrumental resolution. Second, the quasielastic broadening was modeled by a single Lorentzian curve with a width w_{qe} and an integrated area I_{qe}. In all fits, the peak centers were constrained to be the same for each component.

All materials were handled solely under inert Ar or He atmosphere. The samples were loaded in lead sealed flat ($LiBH_4$ and $NaBH_4$) or double-walled cylindrical (KBH_4) Al containers. The 1 mm × 30.0 mm × 40.0 mm sized flat containers were oriented at an angle of 135° with respect to the incident beam. The diameter of the cylindrical container was 10 mm and the wall distance (i.e., the sample space) was 1 mm. A packing density of about 30% was achieved, resulting in a transparency of about 70% for all three samples.

B. Theoretical

The present calculations were performed within periodic plane-wave implementation of DFT approach.[18,19] The valence configurations $1s^1$ for H; $2s^22p^1$ for B; $2s^11s^2$ for Li; $3p^64s^23d^1$ for Na, and $4s^24p^65s^24d^1$ for K were represented by projected augmented wave potentials[20,21] and the generalized gradient approximation (GGA) was used for the exchange-correlation functional.[22] Energy cutoff of 600 eV and k-point grid with spacing of 0.05 Å^{-1} were applied. Atomic positions and unit-cell parameters were relaxed with conjugated gradient algorithm until the forces excerpted on atoms were smaller than 0.005 eV/Å.

The rotational barriers for BH_4 units were determined in $2\times2\times2$ supercells by nudged elastic band (NEB) method.[23,24] For these calculations all but the rotating BH_4 were fixed in their equilibrium positions. Normal-mode analysis was performed for all systems at the ground state and at the transition state by a finite atomic displacements of the order ±0.02 Å. The hopping rate between adjacent orientations was expressed as: $\kappa=\gamma(T)\exp(\frac{-E_A}{k_BT})$, where temperature-dependent prefactor γ equals: $\gamma(T)=\frac{\Pi_i\nu_i f(h\nu_i/2k_BT)}{\Pi_j\nu_j f(h\nu_j/2k_BT)}$. The index i enumerates N normal modes at the ground state, and j is for $N-1$ modes at the transition state. The function $f(x)=\sinh(x)/x$, k_B is the Boltzman constant, T the temperature, and ν is the frequency of a normal mode.[25] For the low-temperature phase of KBH_4 the phonon spectra was calculated in the real space by a set of finite displacements and harmonic approximation.[26,27]

III. RESULTS

A. Rotational motion

In the case of localized jump motion, the *measured* total incoherent-scattering function $S^{inc}_{meas}(Q,\omega)$ can be expressed as the convolution of the elastic line $\delta(\omega)$ and the broader quasielastic line $L(Q,\omega)$, with the resolution function of the instrument $R(Q,\omega)$,

$$S^{inc}_{meas}(Q,\omega)=R(Q,\omega)\otimes[I_{el}(Q)\delta(\omega)+I_{qe}(Q)L(Q\omega)], \quad (1)$$

where I_{el} is the intensity of the elastic line and I_{qe} is the integrated intensity of the quasielastic signal. The quasielastic contribution originates from stochastic motion of hydro-

gen atoms within the sample. It is related to the self-correlation function by Fourier transform and can be expressed by Lorentzian functions L_j,

$$L_j(\omega) = \frac{1}{\pi} \frac{1/\tau_j}{(1/\tau_j)^2 + \omega^2} \tag{2}$$

each with its own width, τ_j. The weight $A_j(Q)$ of the individual L_j is called the *quasielastic incoherent structure factor* $A_j(Q)$. Analogously, the contribution of the elastically scattered neutrons to the signal is called the *elastic incoherent structure factor* $A_0(Q)$ or EISF.

The total incoherent-scattering function can be written as the sum of the elastic and inelastic contributions,[28]

$$S_{tot}^{inc}(Q,\omega) = A_0(Q)\delta(\omega) + \sum A_j(Q)L_j(\omega). \tag{3}$$

If the elastic line and the quasielastic component can be experimentally separated, the EISF is a measurable quantity which can be expressed as

$$A_0(Q) = \frac{I_{el}(Q)}{I_{el}(Q) + I_{qe}(Q)}, \tag{4}$$

where $I_{el}(Q)$ and $I_{qe}(Q)$ are the integrated elastic and quasielastic intensities.

Let us first discuss the measured spectra in a qualitative way, before we deduce the rotational axes, the activation energies and the residence times in more details. For all samples under investigation, no broadening of the elastic line was found for temperatures below 250 K, showing that the hydrogen is frozen in on the time scale accessible by the instrument. At higher temperatures a quasielastic broadening is observed, whose width increases with temperature. Analogous to $NaBH_4$,[29] also for KBH_4 the broadening of the quasielastic contribution with increasing temperature follows an Arrhenius law. At a given temperature, the width of the broadening is independent of Q, indicative of a localized motion. The intensity of the elastic component as well as the EISF approaches zero with increasing Q. We attribute the similar behavior of $NaBH_4$ and KBH_4 to their identical crystalline symmetries. In the case of $LiBH_4$ the situation is different, as shown in Fig. 2. The top panel [Fig. 2(a)] displays a series of spectra for $0.7 < Q < 2.3$ Å^{-1} at $T=380$ K, i.e., within the low-temperature phase while the lower panel [Fig. 2(b)] shows the corresponding spectra measured at $T=400$ K, i.e., in the high-temperature phase. The most obvious difference is the vanishing intensity at higher Q in the high-temperature phase while the scattered intensity remains finite even at higher Q for the low-temperature phase. The phase transition is not only accompanied by different intensities at higher Q but also the width of the Lorentzian contribution suddenly increases as the material transforms into the high-temperature phase.

Figure 3 compares two spectra of $LiBH_4$, recorded at $T=380$ K and at $T=400$ K, both at $Q=1.5$ Å^{-1}, both with 0.20 meV resolution. The two spectra are shifted along the y axis for clarity. Black dots are the measured data points while the black line represents the fit consisting of an elastic line and a quasielastic contribution. Note the increase in the width of the quasielastic component in the high-temperature phase as compared to the low-temperature phase.

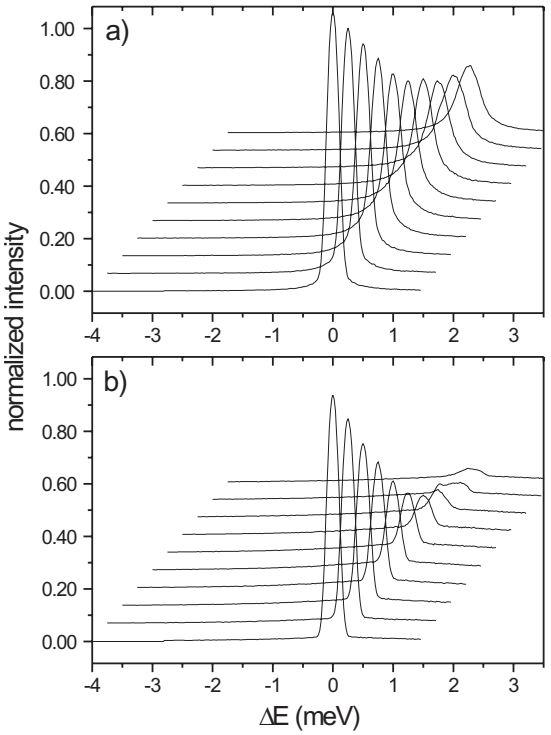

FIG. 2. QENS of $LiBH_4$, measured (a) at $T=380$ K, below the phase transition and (b) at $T=400$ K above the phase transition. The spectra were binned in a range of scattering vectors of $Q=0.5-2.5$ Å^{-1} with $\Delta Q=0.2$ Å^{-1}. The spectra are offset for clarity. The phase transition is characterized by distinct different quasielastic linewidths.

The rotational behavior of the BH_4 units can be described on the basis of their EISFs. Figure 3 displays the experimentally obtained EISFs, extracted from the QENS spectra according to Eq. (4), together with model EISFs describing (i)

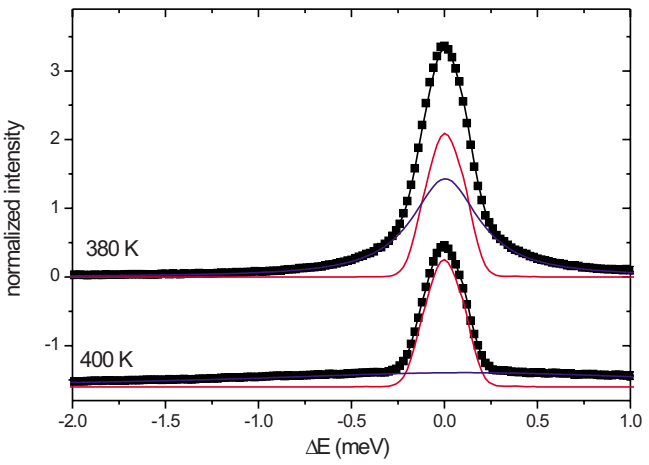

FIG. 3. (Color online) QENS of $LiBH_4$, measured at $T=380$ K (top curve) and at $T=400$ K (bottom curve). Both spectra were recorded at $Q=1.5$ Å^{-1}. The measured data are represented by black symbols. Solid black lines display fits to the data, each one consisting of a resolution limited Delta function (red) and a Lorentzian profile (blue). The spectra are offset for clarity.

90° reorientations of the $(BH_4)^-$ ion around the $c2$ axes (model 1) and (ii) 120° rotations about $c3$ (model 2). The first case is analogous to the reorientations of the isostructural $(NH_4)^+$ ion in ammonium halides, which are classical examples of solid rotor phases.[30] This model has been previously used to describe the rotational reorientations in $NaBH_4$.[29] In this case, the EISF can be expressed as[30]

$$A_0(Q) = \frac{1}{8}[1 + 3j_0(Qa) + 3j_0(Qa\sqrt{2}) + j_0(Qa\sqrt{3})]. \quad (5)$$

The corresponding quasielastic incoherent structure factors $A_j(Q)$ are

$$A_1(Q) = \frac{1}{8}[1 - 3j_0(Qa) + 3j_0(Qa\sqrt{2}) - j_0(Qa\sqrt{3})], \quad (6)$$

$$A_2(Q) = \frac{1}{8}[3 - 3j_0(Qa) - 3j_0(Qa\sqrt{2}) + 3j_0(Qa\sqrt{3})], \quad (7)$$

$$A_3(Q) = \frac{1}{8}[3 + 3j_0(Qa) - 3j_0(Qa\sqrt{2}) - 3j_0(Qa\sqrt{3})], \quad (8)$$

where $j_0(x) = \sin(x)/x$ is the zeroth-order Bessel function and $a = 1.36$ Å is the jump distance, i.e., the edge length of the cube in which the tetrahedron is embedded.

The mean residence time of the BH_4 tetrahedra between two successive arbitrary reorientational jumps τ_{90} is related to the τ_j's from Eq. (2) as

$$\frac{1}{\tau_1} = \frac{2}{\tau_{90}}; \quad \frac{1}{\tau_2} = \frac{4}{3\tau_{90}}; \quad \frac{1}{\tau_3} = \frac{2}{3\tau_{90}}. \quad (9)$$

In the second case, the case of the 120° rotations, the elastic and quasielastic structure factors can be expressed as

$$A_0 = \frac{1}{3}[1 + 2j_0(Qr)], \quad (10)$$

$$A_1 = \frac{2}{3}[1 - j_0(Qr)], \quad (11)$$

where $r = 2$ Å is the jump distance, i.e., the edge length of tetrahedron's edge. In this case, the mean residence time of the BH_4 tetrahedra between two successive arbitrary 120° jumps τ_{120} is given by

$$\frac{1}{\tau} = \frac{3}{2\tau_{120}}. \quad (12)$$

As the size of the BH_4 tetrahedra does not significantly depend on the compound under investigation, only one model curve for each of the two models are plotted in Fig. 4.

Equation (5) nicely reproduces the measured data for $NaBH_4$, KBH_4 and the high-temperature phase of $LiBH_4$. Therefore, we conclude that the BH_4 units in these compounds rotate around the $c2$ axes, analogous to the NH_4 tetrahedra in amonium halides. For the low-temperature phase of $LiBH_4$ the situation is obviously different. In this case the measured EISF does not approach zero for high Q and consequently model 1 fails. The measured data can, however, be described by model 2, as expressed by Eq. (10), which assumes 120° rotational jumps around the $c3$ axes. The data deviate from the models for lower Q and do not extrapolate to unity for $Q \to 0$. We attribute the deviation at lower Q to multiple scattering, which enhances the inelastic part for small angles.

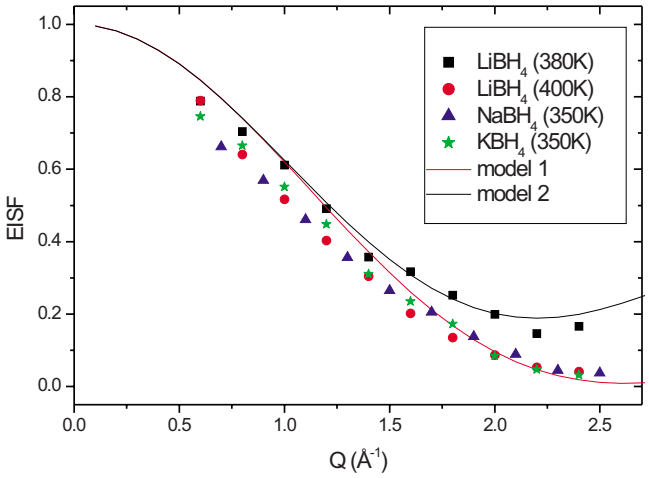

FIG. 4. (Color online) Measured EISFs for the LT phase of $LiBH_4$ (squares), the high-temperature phase of $LiBH_4$ (circles), $NaBH_4$ (triangles), and for KBH_4 (stars). Apart from the LT phase of $LiBH_4$, which was measured at 380 K, all EISF were recorded at 400 K. Solid lines represent model EISFs: Lechner's model of 90° reorientations (model 1), and a three jump model, involving 120° rotations about the $c3$ axis (model 2), respectively.

Each Lorentzian component L_j of the quasielastic broadening is characterized by its individual time constant $\tau_j = 2\hbar/\Gamma$, where Γ is the full width of the corresponding Lorentzian component. The conversion of the τ_j to the residence time is model dependent as described in Eqs. (9) and (12). In principle, for model 1 the quasielastic line should consist of three Lorentzians with different half widths and by Q-dependent amplitudes as expressed in Eqs. (6)–(8). However, the contributions of A_1 and A_2 to the quasielastic intensity are small, only A_3 was considered and the residence times were extracted using τ_3 only. In the case of model 2 the conversion is more straight forward, as only one component exist.

Residence times obey an Arrhenius law: $\tau = \tau_0 \times \exp(E_a/k_BT)$, where k_B is Boltzmann's constant. The Arrhenius fits yield the prefactors τ_0 and the activation energies E_a. Table I lists the experimental values together with the ones obtained by Hagemann *et al.*,[13] measured by Raman spectroscopy.

The measured values of the activation energies for $NaBH_4$ and KBH_4 fit nicely to the values measured by Raman spectroscopy. It should be noted that the value of 15(2) kJ/mol for the HT phase of $LiBH_4$ deduced by Hagemann *et al.*[13] corresponds to a model assuming one energy barrier for the HT phase. Assuming two energy barriers for the HT phase 60(30) kJ/mol and 5(5) kJ/mol were obtained, respectively. In the Raman measurements the energy barrier for the reorientations V is related to the activation energy E_a as derived from QENS or NMR spectroscopy as $V = E_a + h\nu_{vib}$, where

TABLE I. Prefactors τ_0 (in fs) and energy barriers (in kJ/mol) of the rotational motion as derived from QENS (this work) and Raman-scattering experiments (x from Ref. 13). * Calculated values for the high-temperature phases are explained in the text.

Compound	τ_0 (fs)	E_a	E_a^x	E_a (calc.)
$LiBH_4$ (LT)	42(5)	17.3(0.3)		27.0
$LiBH_4$ (HT)	75(15)	6.6(0.5)	15(2)	
$NaBH_4$	31(1)	10.9(0.1)	11.5(0.5)	12.0*
KBH_4	64(3)	9.9 (0.2)	9.2(0.4)	13.5*

ν_{vib} is the libration frequency.[13] Activation energy measurements based on proton spin-lattice relaxation data for $NaBH_4$ and KBH_4 give slightly higher values of 12.2 kJ/mol and 15.5 kJ/mol, respectively.[9] In the LT phase of $LiBH_4$ two types of reorientational motion have been seen by NMR with activation energies of 17.5 and 24.1 kJ/mol.[31]

Figure 5 shows the experimentally obtained data together with the Arrhenius fit in the temperature range from 250 to 550 K. The error bars represent the scatter of the width of the Lorentzian contributions around their respective mean value. Note the discontinuity of the $LiBH_4$ data at the phase transition at 380 K.

B. Phonon density of states

While the quasielastic part of the spectra yields information about the stochastic motion of single particles, the inelastic spectra measure collective motions. Due to the large incoherent-scattering cross section of hydrogen mainly the hydrogen PDOS is measured. The measured PDOS of KBH_4 in the temperature range of 100–500 K together with the

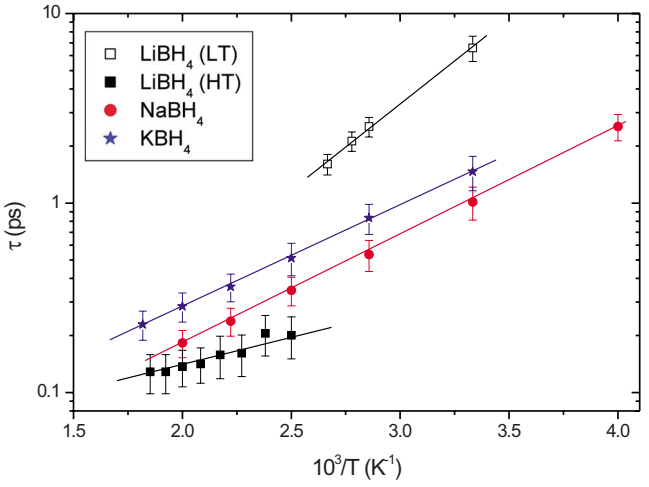

FIG. 5. (Color online) Thermally activated Arrhenius behavior of the rotational motion. The time τ corresponding to the inverse width of the quasielastic broadening can be expressed as $\tau = \tau_0 \exp(E_a/k_BT)$. The prefactors and activation energies are listed in Table I. Open squares refer to the low-temperature phase of $LiBH_4$, closed squares to the high-temperature phase of $LiBH_4$, circles to $NaBH_4$, and stars to KBH_4.

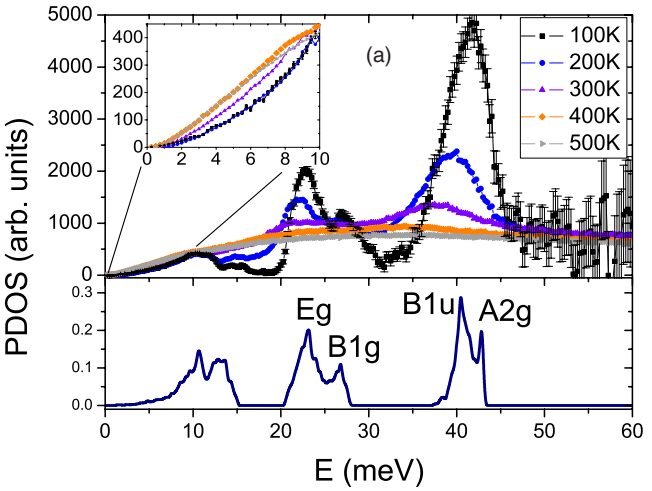

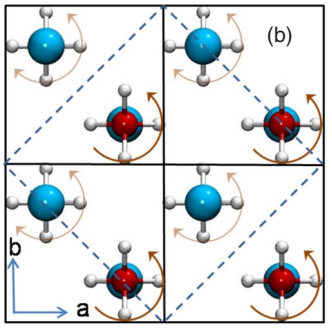

FIG. 6. (Color online) (a) PDOS of hydrogen for KBH_4 for temperatures between 100 and 500 K. The inset shows an enlargement for energies below 10 meV. A calculated phonon spectrum for the low-temperature phase of KBH_4 is shown in the bottom part of the plot. (b) Schematic view of B1u and A2g librational mode displacements. Large light (blue) spheres represent K, small dark (red) represent B, and white ones H. The arrows indicate the directions of the collective motion of BH_4. Bold arrows indicate rotation of BH_4 groups in the upper layer while thin arrows show the rotation of the subsequent layer in c direction. For the A2g mode the BH_4 groups on consecutive layers rotate in phase and for B1u in antiphase.

PDOS calculated for the low-temperature phase of KBH_4 are depicted in Fig. 6(a). As the spectra of the isostructural $NaBH_4$ and KBH_4 are similar, we restrict our discussion to KBH_4. For the case of $LiBH_4$, the only alkaline borohydride with a different crystal structure, the PDOS has been discussed elsewhere.[3,32] The strongest peak in the spectrum of KBH_4 at 40 meV originates from degenerated infrared (Eu), raman (Eg), and from two librational (B1u and A2g) modes. Atomic displacements related to librational modes are presented in Fig. 6(b). The second strongest peak at 23 meV corresponds to an infrared and raman optical lattice mode. The broad feature around 10 meV can be identified as the acoustic-mode frequencies.[33] The low-temperature phonon spectra remains visible well above the phase-transition temperature, indicating that the local ordering of BH_4 is present also in the cubic phase of KBH_4.

With increasing temperature the peaks broaden and shift to lower energies. The shift is a result of thermal lattice expansion while the broadening is a sign of reduced correlation length. A broad librational mode at room temperature has

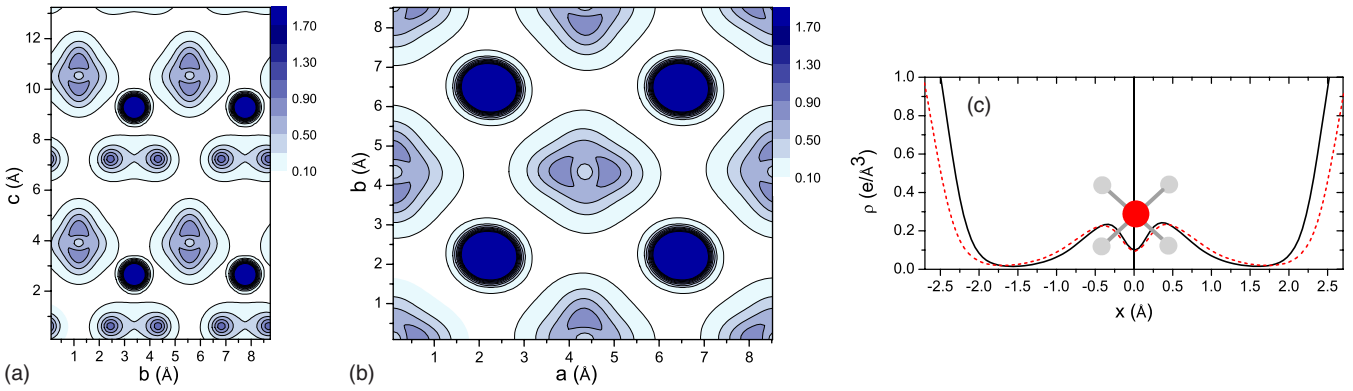

FIG. 7. (Color online) The cross section of the charge density at boron plane for the low-temperature *Pnma* phase of $LiBH_4$ (a), and for the high-temperature phase of $NaBH_4$ (b), and along the line between potassium, boron, potassium for KBH_4 (c). The cross section is cut along the (b,c) crystallographic plane for $LiBH_4$ and (a,b) crystallographic plane for $NaBH_4$. The dark circles represent charge density at metal atoms, the scale for density in electron per cubic angstrom is given on the right side of the plots. In (c) a schematic view of the BH_4 group is shown in the middle, with boron as darker (red) sphere in the center and hydrogen atoms as light gray circles.

also been observed for $RbBH_4$ and $CsBH_4$ (Ref. 33) as well as for ammonium salts[34] and for bisulphide salts.[35] In all cases the system undergoes librations in a harmonic potential at low temperature, then proceed at higher temperatures to a transition region where the ion librates and eventually makes a rotational jump. Finally, at even higher temperatures, the system reaches the free rotor state. We clearly observe the intermediate, hindered rotor state.

At low energies, the PDOS at temperatures up to 200 K depends quadratically on the phonon energy as expected by the Debye theory for acoustic vibrations in crystalline solids, as shown in the inset of Fig. 6. This feature is basically temperature independent for energies below 10 meV. At higher temperatures, with the onset of the rotational motion, the slope of the PDOS changes toward a linear behavior, which is reached at 400 K. The PDOS recorded at 300 K shows a slope that lies in between the linear and the quadratic one. Compared to the PDOS given by the Debye theory, the excess of low-energy density of states at high temperature reveals lattice anharmonicities and is a characteristic feature of glasses and disordered systems.[36,37] We attribute the continuously increasing disorder to the enhanced rotational motion at increasing temperature. Note that in the case of $NaBH_4$ and KBH_4, the disorder evolves within their respective high-temperature phases. $LiBH_4$ on the other hand shows a sudden change from the ordered (quadratic PDOS) to the disordered (linear PDOS) state at the structural phase transition.[3] It seems that the increase in unit-cell volume, which is associated with the phase transitions in $NaBH_4$ and KBH_4 releases the $c2$ rotation.

C. Theoretical results

While the structural properties of the ordered room-temperature phase of lithium borohydride can be calculated with reasonable accuracy,[3,38,39] the disordered room-temperature phases of sodium and potassium borohydride require special attention. These structures include lattice sites with an occupancy 0.5 for hydrogen that cannot be considered directly in the DFT approach as this method requires to specify the lattice positions for all atoms. The partial occupancy results from the dynamical hopping of the BH_4 subunits between symmetry allowed orientations. The static structures as used for the calculations represent an instant snapshot for one particular configuration. Specifically, we optimized structures for KBH_4, which is isostructural to $NaBH_4$, in the high-temperature phase. Four different structures were considered in the cubic $Fm\bar{3}m$ unit cell, the fully ordered BH_4 structure (all possessing the same orientation), those with perpendicular orientation of BH_4 in the (a,b) plane, and with antiparallel orientation along the c direction. These resulting final structures differ in energy by $\sim$0.1 eV/f.u. The lowest-energy structure has the smallest specific volume per formula unit (70.33 Å^3/f.u.) while the fully ordered structure possesses the highest energy and has a specific volume 70.90 Å^3/f.u. The calculated volumes are about 2% smaller than the experimentally determined one. The underestimation of the lattice parameter (or the overbinding) by DFT calculation is a consequence of the "static" calculation, neglecting the entropy terms arising from dynamic disorder. However, for the sake of clarity, we focused our attention on the fully ordered structure.

We first consider the charge density, originating from the valence charges of the metal and BH_4 ions. The two-dimensional cross sections of the charge density for $LiBH_4$ and $NaBH_4$ are presented in Figs. 7(a) and 7(b). For $LiBH_4$ the molecular $c2$ symmetry axis does not match the m mirror plane crystalline symmetry at site $4b$ of the boron atom; thus the local-field forces rotations of BH_4 around axes that are different from the high-symmetry axes of the BH_4 tetrahedron, as shown in Fig. 7(a).

For sodium borohydride, the site symmetry $(m\bar{3}m)$ for boron located at the $4c$ lattice site is in accordance with the $c2$ symmetry of the BH_4 group when the crystal field originated from nearest metal cations is considered [see Fig. 7(b); for KBH_4 the picture is similar]. However, the presence of the BH_4 second neighbors breaks the fourfold symmetry as long as only the static configurations of BH_4 groups without partial occupancy are considered. This is a reason for distinct two minima related by 90° rotation, as reported previously.[29]

In the structure where all sites for hydrogen are occupied (time average) $m\bar{3}m$ site symmetry is conserved and two possible orientations of BH_4 (connected by 90° rotation) are equivalent.

As the properties of metal borohydrides are determined to a great extend by electrostatic interactions between the metal cations and the BH_4 anions,[38] in Fig. 7(c), the valence charge density along the line connecting two metal cations and passing through boron is depicted on the example of KBH_4. The charge density is presented for the structure optimized at the ground state, (black solid line); and for structure that is expanded by 2% with respect to the optimized one. For the expanded structure the slope of charge-density decay is smaller, reducing the field gradients and finally lowering the effective barriers for rotation of the BH_4 groups.

For the structure that results from geometry optimization two distinct minima can be observed [similar as for $NaBH_4$ (Ref. 29)]. However, if the structure is expanded to match the experimental lattice parameters, the potential-energy landscape becomes significantly flatter and distinction between minima is less pronounced. The optimized geometry results from the electrostatic attraction between ions, and do not include any effects related to configurational entropy. This results in "overbinding" for structures of borohydrides in DFT calculations, and give an incorrect picture for molecular rotation[38] that require rather free-energy landscape.

The height of the rotational barriers and the preferred rotation axes can be calculated by nudged elastic band method.[23,24] For $LiBH_4$ the barrier for BH_4 rotation around the initial $c2$ axis equals 27 kJ/mol. In agreement with Ikeshoji *et al.*, the actual rotation axis is not parallel to any of the high-symmetry axes of BH_4.[14] This is a significantly larger value than the measured barrier, Table I, that can be explained by underestimation of the specific volume by DFT calculations of this compound. In general GGA approximation overestimates the lattice parameters[40] for simple solids while for metal borohydrides the lattice parameters are usually underestimated. One of the reasons for this overbinding is due to overlooking of the BH_4 hopping motion that occurs even at relatively low temperatures.

For $NaBH_4$ the barrier for rotation around $c2$ axis is 19.3 kJ/mol for the static structure that is optimized at the ground state, however, expansion of the lattice parameters by 5% lowers the calculated barrier to 12.0 kJ/mol. This compares favorably to values measured by scattering methods. For KBH_4 we have calculated barriers for BH_4 rotation around $c2$ axis for three structures: those with optimal lattice parameters at the ground state, the one with lattice expanded by 2% to match experimental values, and the lattice expanded by 5%. The barriers are 23.1 kJ/mol, 18.8 kJ/mol, and 13.5 kJ/mol, respectively. For both compounds NEB method gives $c2$ axis as the most favorable rotation axis for BH_4.

Analysis of the normal modes at the ground state and at the transition state provides information about the prefactor in the Arrhenius picture, thus allows direct comparison of the measured and calculated rotational motion. Prefactors are: 243.8 fs, 154.3 fs, and 160.1 fs for borohydrides of Li, Na, and K, respectively, at 400 K. The static activation energies (hopping barriers) are shown in Table I. For the high-temperature phases of $NaBH_4$ and KBH_4 barriers are calculated for lattice expanded by 5% with respect to static ground-state configuration. For smaller lattice these barriers are larger and they equal 19.3 kJ/mol for $NaBH_4$ and 23.1 kJ/mol for KBH_4.

The calculated PDOS for KBH_4 reproduces all the features observed at 100 K (see Fig. 6). It is interesting to note that even though the calculations have been carried out for the low-temperature phase, they persist in the higher-temperature phase, where the lattice is expanded [in Figs. 6(a) and 6(b)]. This expansion releases rotation around $c2$. As the temperature rises, the correlation length drops down and the observed peaks vanish.

IV. DISCUSSION

In the present paper we have studied rotational motion of BH_4 molecular groups by means of quasielastic and inelastic neutron-scattering and density functional calculations. We show that on the macroscopic time-scale BH_4 units are mobile in all studied compounds. The motions are thermally activated and characterized by activation energies in the order of 0.1 eV, typical frequencies are in the terahertz range at temperatures of about 400 K. Thereby the crystal structure, more specifically the electrostatic interactions between the constituent ions determine the axis of rotation. In the orthorhombic low-temperature phase of $LiBH_4$ the BH_4 tetrahedra rotate about their threefold $c3$ axes while their reorientations in the hexagonal high-temperature phase of $LiBH_4$ and in the cubic room-temperature phases of $NaBH_4$ and KBH_4 occur around their twofold $c2$ axes. The energetic barriers for the rotation are of the same order of magnitude for $NaBH_4$ and KBH_4 while they are considerably smaller for the high-temperature $LiBH_4$ phase, see Table. I. The barriers for rotation were also calculated within DFT, where the disordered fcc structures of $NaBH_4$ and KBH_4 were approximated by a static ordered configuration, with the lattice expanded to the experimental value. Despite these approximations, the hopping barriers can be calculated with reasonable agreement with the experimental data. The calculated prefactors, however, differ by about one order of magnitude with respect to the measured ones as shown in Table I. This is related to the harmonic treatment of transition state theory that considers rotational jumps as independent events. However, lattice anharmonicity is indeed present and has been measured by inelastic neutron scattering that show a continuous increase in this effect with increasing temperature.

Within the ionic crystal of metal borohydrides, the $(BH_4)^-$ anion achieves a stable, eight-electron closed-shell configuration. Within the BH_4 ion, the negative charge is carried by the hydrogen. Apart from the charge transfer from the metal, there is an additional electron transferred from the B to the H, so that each H carries a charge of about 1.5 electrons.[38,41] The structure, local static, and dynamical properties of BH_4 groups are determined by electrostatic interaction between ions in the crystal.[38] Especially, in strongly ionic compounds such as $LiBH_4$, $NaBH_4$, or KBH_4 mutual orientation of BH_4 with respect to metal cations (local structure) depends on the charge transfer. The monodentate (single hydrogen pointing

toward metal cation) orientation is energetically strongly unfavorable while two or three hydrogen atoms pointing toward metal are competitive in the energy scale.

In the cubic phases of $NaBH_4$ and KBH_4, the orientation of the $c2$ axes along the $\langle 100 \rangle$ directions results in a bidentate configuration. During a $c2$ rotation the tetrahedron keeps the bidentate configuration while a $c3$ rotation involves an unfavorable monodentate intermediate state. Thus the energy landscape of $NaBH_4$ and KBH_4 displays large barriers for $c3$ rotation and smaller barriers for $c2$ rotation.[29] Due to symmetry there are two possible orientations of BH_4 tetrahedron in the lattice that are equally occupied on the macroscopic time scale giving site occupancy 0.5 for hydrogen.

In the orthorhombic low-temperature phase of $LiBH_4$ the situation is different. The $c2$ rotation axes do not coincide with any symmetry operation of the lattice. In this compound the separation between nearest boron atoms is $d_{B\text{-}B} \sim 3.8$ Å, (much smaller than $d_{B\text{-}B} \sim 4.25$ Å, for $NaBH_4$, or $d_{B\text{-}B} \sim 4.63$ Å, for KBH_4). As presented in Refs. 3 and 29 the potential-energy surface for BH_4 rotation possesses four local minima for rotation around $c2$ axis for borohydrides of sodium and potassium. In Fig. 7(b) the distribution of static charge density clearly shows that BH_4 orientation related by 90° rotations are not equivalent with respect to the nearest neighbors of the same molecular groups (in given crystallographic plane). As a result local potential-energy minima related to orientation are different. This difference decreases with increasing separation between anions, Fig. 7. For $LiBH_4$, the tetrahedra are arranged with alternating orientations that results from lattice symmetry and close proximity of boron atoms. Consequently this structure does not possesses disorder and the barriers in the calculated potential-energy landscape are higher along the $c2$ axes than along the $c3$ axes.[3]

To summarize, we investigated the rotational motion of the BH_4 units in alkali borohydrides by means of combined quasielastic neutron-scattering and DFT calculations. Within the ionically bound alkali borohydrides, the BH_4 anions are not fixed, they undergo thermal activated rotational jumps in the terahertz regime with activation energies in the order of 0.1 eV. The axis of rotation is determined by symmetry, the electrostatic interactions and the distances within the crystal. The experimentally obtained results can be understood on the basis of DFT calculations, especially the barrier height and the potential-energy landscape.

ACKNOWLEDGMENTS

This work is based on experiments performed at the Swiss spallation neutron source SINQ, Paul Scherrer Institute, Villigen, Switzerland. Financial support from the Swiss National Science Foundation (SNF-Project No. 200021-119972/1) is gratefully acknowledged. Z.L. kindly acknowledges partial support by MNiSW Project No. N202 207138.

*arndt.remhof@empa.ch; http://www.empa.ch/h2e

†Also at Physical Chemistry, Saarland University, D-66123 Saarbrücken, Germany.

[1] B. H. Liu and Z. P. Li, J. Power Sources **187**, 291 (2009).

[2] A. Züttel, A. Borgschulte, and S.-I. Orimo, Scr. Mater. **56**, 823 (2007).

[3] F. Buchter, Z. Łodziana, Ph. Mauron, A. Remhof, O. Friedrichs, A. Borgschulte, A. Züttel, D. Sheptyakov, T. Strässle, and A. J. Ramirez-Cuesta, Phys. Rev. B **78**, 094302 (2008).

[4] P. Fischer and A. Züttel, Mater. Sci. Forum **443-444**, 287 (2004).

[5] G. Renaudin, S. Gomes, H. Hagemann, L. Keller, and K. Yvon, J. Alloys Compd. **375**, 98 (2004).

[6] F. Buchter, Z. Łodziana, A. Remhof, O. Friedrichs, A. Borgschulte, Ph. Mauron, A. Züttel, D. Sheptyakov, G. Barkhordarian, R. Bormann, K. Chłopek, M. Fichtner, M. Sørby, M. Riktor, B. Hauback, and S. Orimo, J. Phys. Chem. B **112**, 8042 (2008).

[7] Y. Filinchuk, H. Hagemann, Eur. J. Inorg. Chem. **2008**, 3127 (2008).

[8] P. Martelli, R. Caputo, A. Remhof, Ph. Mauron, A. Borgschulte, and A. Züttel, J. Phys. Chem. C **114**, 7173 (2010).

[9] O. A. Babanova, A. V. Soloninin, A. P. Stepanov, A. V. Skripov, and Y. Filinchuk, J. Phys. Chem. C **114**, 3712 (2010).

[10] M. Hartman, J. Rush, T. Udovic, R. Bowman, Jr., and S.-J. Hwang, J. Solid State Chem. **180**, 1298 (2007).

[11] C. C. Stephenson, D. W. Rice, and W. H. Stockmayer, J. Chem. Phys. **23**, 1960 (1955).

[12] J.-Ph. Soulié, G. Renaudin, R. Černý, and K. Yvon, J. Alloys Compd. **346**, 200 (2002).

[13] H. Hagemann, S. Gomes, G. Renaudin, and K. Yvon, J. Alloys Compd. **363**, 129 (2004).

[14] T. Ikeshoji, E. Tsuchida, K. Ikeda, M. Matsuo, H.-W. Li, Y. Kawazoe, and S.-I. Orimo, Appl. Phys. Lett. **95**, 221901 (2009).

[15] J. Mesota, S. Janssen, L. Holitzner, and R. Hempelmann, J. Neutron Res. **3**, 293 (1996).

[16] S. Janßen, J. Mesot, L. Holitzner, A. Furrer, and R. Hempelmann, Physica B **234-236**, 1174 (1997).

[17] http://www.ncnr.nist.gov/dave

[18] G. Kresse and J. Furthmüller, Comput. Mater. Sci. **6**, 15 (1996).

[19] G. Kresse and J. Furthmüller, Phys. Rev. B **54**, 11169 (1996).

[20] P. E. Blöchl, Phys. Rev. B **50**, 17953 (1994).

[21] G. Kresse and D. Joubert, Phys. Rev. B **59**, 1758 (1999).

[22] J. P. Perdew, K. Burke, and M. Ernzerhof, Phys. Rev. Lett. **77**, 3865 (1996).

[23] G. Henkelman, B. Uberuaga, and H. Jònsson, J. Chem. Phys. **113**, 9901 (2000).

[24] G. Henkelman and H. Jònsson, J. Chem. Phys. **113**, 9978 (2000).

[25] D. S. Sholl, J. Alloys Compd. **446-447**, 462 (2007).

[26] Z. Łodziana and K. Parliński, Phys. Rev. B **67**, 174106 (2003).

[27] A. Togo, F. Oba, and I. Tanaka, Phys. Rev. B **78**, 134106 (2008).

[28] J. D. Barnes, J. Chem. Phys. **58**, 5193 (1973).

[29] A. Remhof, Z. Łodziana, F. Buchter, P. Martelli, F. Pendolino, O. Friedrichs, A. Züttel, and J. P. Embs, J. Phys. Chem. C **113**, 16834 (2009).

[30] R. E. Lechner, G. Badurek, A. J. Dianoux, H. Hervet, and F. Volino, J. Chem. Phys. **73**, 934 (1980).
[31] A. V. Skripov, A. V. Soloninin, Y. Filinchuk, and D. Chernyshov, J. Phys. Chem. C **112**, 18701 (2008).
[32] R. Gremaud, A. J. Ramirez-Cuesta, K. Refson, D. Colognesi, A. Züttel, and A. Borgschulte (unpublished).
[33] J. Tomkinson and T. Waddington, J. Chem. Soc., Faraday Trans. 2 **72**, 528 (1976).
[34] V. Brajovic, H. Boutin, G. J. Safford, and H. Palevsky, J. Phys. Chem. Solids **24**, 617 (1963).
[35] P. T. Ford, Discuss. Faraday Soc. **19**, 230 (1955).
[36] S. R. Elliott, *Physics of Amorphous Materials* (Longman Scientific and Technical, Harlow, Essex 1990).
[37] G. Parisi, J. Phys.: Condens. Matter **15**, S765 (2003).
[38] Z. Łodziana and M. J. van Setten, Phys. Rev. B **81**, 024117 (2010).
[39] Z. Łodziana, A. Züttel, and P. Zielinski, J. Phys.: Condens. Matter **20**, 465210 (2008).
[40] S. Kurth, J. P. Perdew, and P. Blaha, Int. J. Quantum Chem. **75**, 889 (1999).
[41] F. Buchter *et al.* (unpublished).